INTERNATIONAL JOURNAL OF OPTIMIZATION IN CIVIL ENGINEERING
Int. J. Optim. Civil Eng., 2025; 15(4):557-571

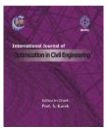

SEISMIC IMPROVEMENT OF LOW-RISE BUILDINGS USING OPTIMUM VARIABLE AND FIXED RADIUS FRICTION PENDULUM ISOLATOR

R. Kamgar, H. Pooladi Baghbadorani, and H. Heidarzadeh[*,†]
[1]*Department of Civil Engineering, Shahrekord University, Shahrekord, Iran*

ABSTRACT

Controlling vibrations in short-period structures subjected to seismic loading is crucial for improving the seismic performance of the structure. This paper investigates friction pendulum isolators with both constant and variable radius as a means to enhance the seismic behavior of structures. Friction pendulum isolators with a constant radius are susceptible to intensification phenomena in near-field earthquakes. Modifying the isolator radius leads to changes in its period and stiffness, thereby mitigating the amplification effect. The study first models and validates the friction pendulum isolator with a constant radius using ABAQUS software. Subsequently, the performance of these isolators, both with constant and variable radius, is examined under harmonic loading to improve structural behavior. The results show that variable radius pendulum friction isolators have been able to increase energy absorption by an average of 25%, 41%, and 14%, respectively, in response to near- and far-field earthquakes such as the Manjil, Loma Prieta, and Northridge earthquakes. This reduces the transfer of earthquake forces to the structure and maintains the integrity of the structure during an earthquake.

Keywords: Seismic performance; Friction pendulum isolators; Fixed and variable radius; Lateral loading.

Received: 28 September 2025; Accepted: 13 November 2025

1. INTRODUCTION

Seismic isolators are actually equipment for seismic control of structures that replace the rigid connection of the structure to the foundation and are used to reduce the transfer of force from the ground to the structure when an earthquake occurs. Isolators cause the

[*]Corresponding author: Department of Civil Engineering, Shahrekord University, Shahrekord, Iran
[†]E-mail address: heidarzadeh@sku.ac.ir (H. Heidarzadeh)

displacement of the structure to be concentrated at the isolated level and reduce the displacement of the structure's floors under the influence of earthquake forces. Isolators also reduce excessive deformations in structural and non-structural elements, and in this way, the designer will achieve a more appropriate safety margin against earthquakes.

The idea of base isolation as a method of earthquake-proofing structures began in the last century. Among the first serious studies in the field of isolation is that of John Mylen. John Mylen (1886) at the University of Tokyo successfully constructed a model of an isolated building by placing it on cast-iron balls and piles with rounded edges. In this design, cast iron plates were attached to the building at the top of the balls and, except for a slight concavity, were the same as the plates below. He realized that his design was not strong enough and performed properly against wind forces, so he made changes and modifications to his isolation system to achieve the desired stability against wind forces and tested his final design during a real earthquake, with the result being successful [1].

Today, the construction industry is one of the most vital aspects of human life. Earthquake-induced damage in this domain has prompted engineers to conduct a more detailed examination of the characteristics of severe ground motions and their impact on structural performance. The aim is to design structures with an appropriate response to earthquakes and reduce vulnerability. Therefore, precise and suitable design and configuration are necessary to ensure structures demonstrate acceptable resilience. One common approach is to enhance structural resistance against earthquake forces. In other words, various engineering methods are employed to retrofit and strengthen structures in response to the fundamental human need for safety in buildings [2-4]. From an engineering perspective, retrofitting is not solely about increasing a structure's resistance to earthquakes. Still, it primarily focuses on improving the performance and response of structural elements to the forces imposed during earthquakes.

Given these considerations, retrofitting has gained increased significance among engineers, particularly in the domain of seismic forces, where seismic retrofitting has become a focal point of attention. One innovative method in seismic retrofitting is the utilization of base isolators. The goal is to separate the structure's foundations from the ground, departing from traditional retrofitting methods. These devices typically possess two key features: flexibility and the ability to dissipate energy. The flexibility feature enhances the primary period of the structure, allowing it to exceed the detrimental energy range of seismic forces.

Additionally, energy dissipation properties contribute to increased damping and reduced displacement variations resulting from flexibility. Friction-based isolators, particularly pendulum friction isolators, are among the most common types capable of controlling floor accelerations and deformations. Integrating appropriate isolator systems, along with suitable materials and construction methods at the early stages of structural design, can easily provide the necessary safety margins for the structure. A seismic isolator system can adjust its stiffness and damping during motion, enabling optimal performance across a range of seismic intensity levels [5].

Friction pendulum isolators leverage the friction and velocity variances between system components to enhance their performance. Operating in a sliding manner, these isolators employ a slider and a concave surface. Their governing principles are rooted in the dynamics of a pendulum and the effects of stable friction. In this system, friction plays a

crucial role as the primary energy dissipation mechanism during seismic events. Optimizing friction parameters, such as the friction coefficient and material properties, enhances the system's overall performance.

Generally, the friction pendulum isolator, owing to its simple structure and dependence on pendulum dynamics and friction effects, plays a significant role in improving the performance of seismic mitigation systems. The principles governing isolators with a constant radius are analyzed based on the equations of angular motion of the pendulum and friction effects. These principles serve as the foundation for the precise analysis of this system's performance. The constant radius plays a key role in regulating dynamic motion and energy exchange with the structure. Moreover, single-surface friction isolators with constant curvature have been examined as an essential approach. These isolators may exhibit limitations under specific conditions. To address these issues, suggestions for their modification and improvement have been proposed.

One of the emerging types of friction isolators is that with variable curvature, which operates differently from its constant curvature counterparts. These isolators, with their changing curvature, exhibit variable oscillation periods and frequencies, enabling them to be used effectively in different conditions [2, 3].

This research employs analytical and numerical methods to model the behavior of seismic isolators with constant and variable radii under harmonic loading. Parameters such as displacement range and resisting force were evaluated and compared. Results indicate that isolators with variable radii exhibit superior seismic performance compared to those with constant radii. Consequently, it is recommended to use optimized seismic isolators with variable radii to enhance safety and reduce the vulnerability of structures against seismic events.

2. THE FORCE-DISPLACEMENT RELATIONSHIP OF FRICTION PENDULUM ISOLATORS

Based on studies conducted by Constantino in 2004, as well as Fenz and Constantino in 2008 [6], this section examines the calculation procedure related to the force-displacement relationship of friction pendulum isolators. Referring to the free-body diagram of the isolator depicted in Fig. 1 and writing the equilibrium equations in the horizontal and vertical axes, Eqs. (1-2) are derived, respectively. From the geometry, "u" is defined as the horizontal displacement of the point corresponding to the center of the sliding rotation, representing the radial distance between the center of curvature of the sliding spherical surface and the center of rotation. This distance can be defined using Eq. (3), where "r" is the radius of curvature of the sliding surface, by combining Eqs. (1-3), the force-displacement relationship of the friction pendulum isolator is obtained, as expressed in Eq. (4). In many cases, the radius of curvature of the sliding surface is significantly larger than the horizontal displacement, allowing the simplification of the relationship to the final form presented in Eqs. (5-6) [6].

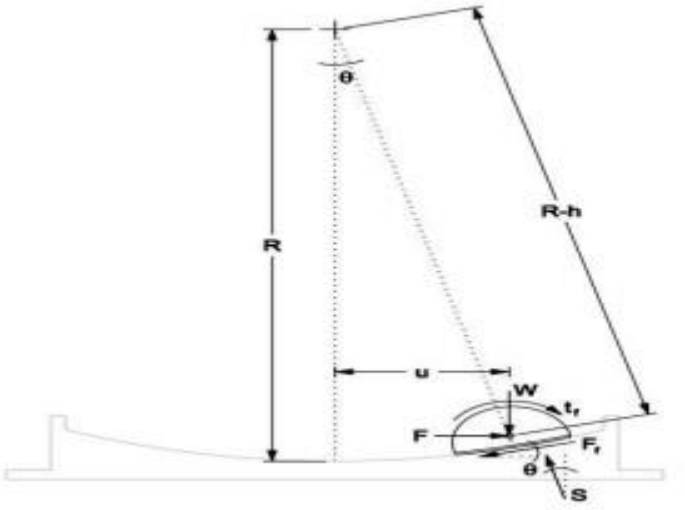

Figure 1: Free-body diagram of the friction pendulum isolator

$$F - S \times \sin\theta - F_f \times \cos\theta = 0 \tag{1}$$

$$W - S \times \cos\theta + F_f \times \sin\theta = 0 \tag{2}$$

$$u = (R - h) \times \sin\theta = R_{eff} \times \sin\theta \tag{3}$$

$$F = \left(\frac{W}{R_{eff}} \right) \times u + \frac{F_f}{\cos\theta} \tag{4}$$

$$F = \left(\frac{W}{R_{eff}} \right) \times u + F_f \tag{5}$$

$$F_f = \mu W \tag{6}$$

2.1. Equations of motion for friction pendulum isolator with variable radius on an elliptical base

According to the studies and research conducted by Sinha and Pransh, if the isolator has a sliding surface based on an elliptical equation where "*a*" is the major semi-axis and "*b*" is the minor semi-axis, the following relationships hold:

$$y = b\left(1 - \sqrt{(1 - \frac{x^2}{a^2})} \right) \tag{7}$$

In Eq. (7), "*a*" represents a linear function of the displacement "*u*", defined by the relationship given in Eq. (8).

$$a(x) = x + d \tag{8}$$

In Eq. (7), the parameter "*d*" is a constant. Considering the above equations, Eqs. (8-9) are obtained.

$$y = b\left(1 - \frac{\sqrt{d^2 + 2\times d\times|x|}}{d+|x|}\right) \tag{9}$$

$$F(x) = mg\times\left(b\left(-\frac{x\times d}{|x|(d+|x|)\sqrt{d^2+2\times d\times|x|}} + \frac{x\times\sqrt{d^2+2\times d\times|x|}}{|x|\times(d+|x|)^2}\right)\right) + \mu\times mg \tag{10}$$

In the above equations, "m" represents the mass acting on the upper plate, and "μ" is the coefficient of friction between surfaces [7].

3. VALIDATION

3.1. Validation of single-surface friction pendulum isolator with constant radius

For the validation of the isolator, Abaqus software has been utilized. Abaqus is a simulation and analysis software for mechanical and solid structures developed by Simulia. Using the modules of this software, each component has been created and assembled based on the dimensions and sizes provided in Fig. 2. Mechanical properties and characteristics have been assigned to the components according to Table 1.

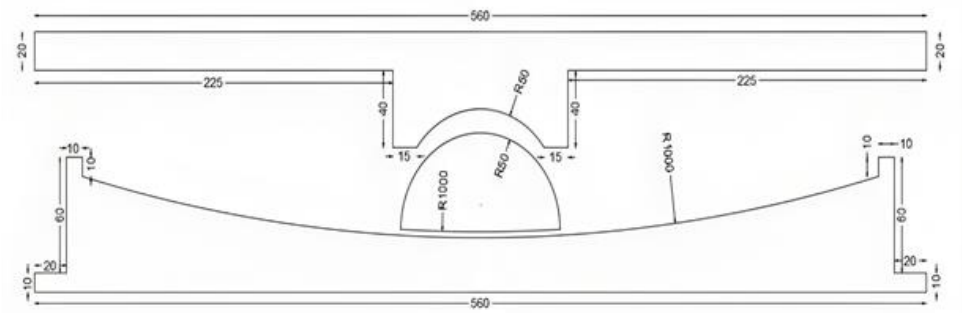

Figure 2: Schematic of the three-dimensional state of the isolator - Two-dimensional dimensions of isolator components

Table 1: Properties and specifications of materials and used components

Parameter	Unit	Value
Density	Kg/m^3	7845
Elastic Modulus	MPa	210000
Poisson's Ratio	-	0.3

In the definition of the solver and the time steps, the General Static analysis approach has been employed. Additionally, for loading the friction pendulum isolator, a constant vertical force is applied to the upper plate, as shown in Fig. 3, where the parameter "RF1" represents

the reaction force due to the friction, and the parameter "RF2" denotes the weight forces of the columns. A sinusoidal lateral displacement cycle is also applied to the bottom plate according to Fig. 4. The modeling has utilized the hexahedral meshing technique with 10-node elements (see Fig. 5).

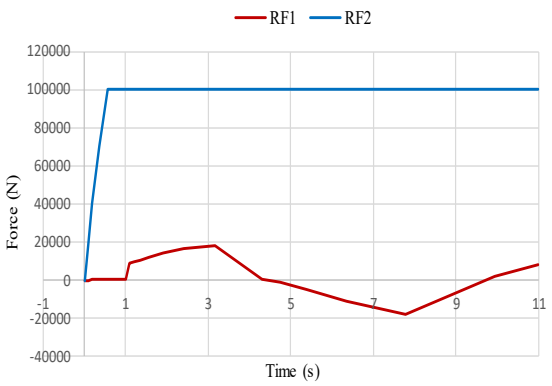

Figure 3: Diagram of forces acting on the isolator

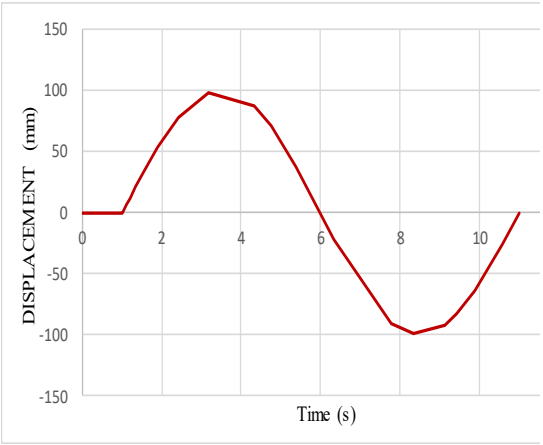

Figure 4: Displacement cycle diagram of the isolator

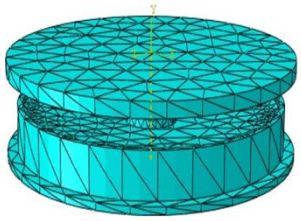

Figure 5: Two-dimensional and three-dimensional schematic of the separator

After creating a suitable job for simulation and analysis, the modeling and simulation were performed using ABAQUS software. Subsequently, the output hysteresis loop is obtained from the friction pendulum isolator model with a constant radius using the available theoretical relationships for examination and comparison [6].

$$F^{+}_{Theory} = (\frac{W}{R_{eff}}) \times u + \mu W \tag{11}$$

$$F^{-}_{Theory} = (\frac{W}{R_{eff}}) \times u + \mu W \tag{12}$$

The parameters considered include "$W = 10^6\ (N)$" the weight acting on the upper surface of the isolator, " $R_{eff} = 1000\ (mm)$ " the curvature radius parameter, " $-100 \le u \le 100\ (mm)$ "the displacement parameter, and "$\mu = 0.08$" the coefficient of

friction between surfaces.

3.2. Comparison of the software results of the isolator with the existing theoretical relationships

The results obtained from the software are well-aligned with the existing theoretical relationships, confirming the credibility of the modeling (see Fig. 6). In this section, the software modeling of the single-surface isolator with a constant curvature has been addressed. By comparing the force-displacement diagram obtained from the software modeling with the diagram derived from theoretical relationships, the accuracy of the software modeling has been evaluated. This final assessment indicates that the software modeling has been conducted with sufficient precision and accuracy.

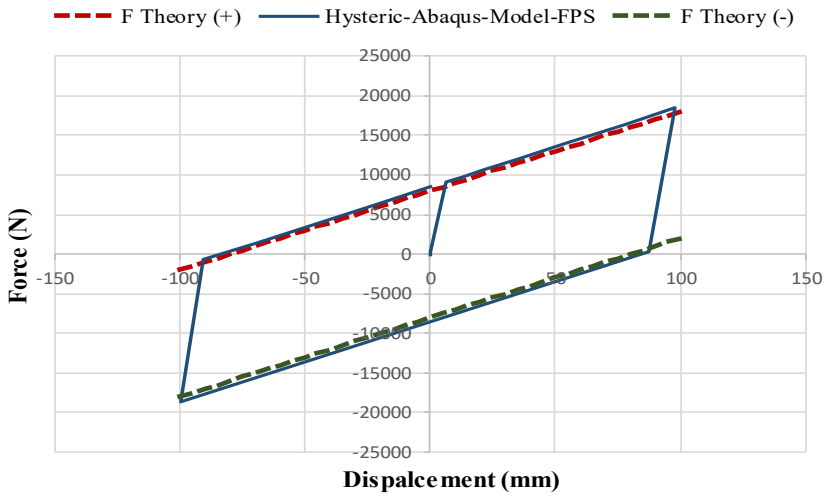

Figure 6: Comparison of the hysteresis behavior diagram output from the software and existing theoretical relationships

4. FRICTION PENDULUM ISOLATOR WITH VARIABLE RADIUS

4.1. Friction pendulum isolator with variable radius on an elliptical base

The variable radius pendulum friction separators are modelled here based on the elliptic equation and are subjected to the displacement-time diagram of Fig. 4. By examining the results obtained according to the software figure and comparing the resulting graphs, it can be concluded that these separators exhibit variable frequencies with changing displacement and stiffness, which indicates their adaptability. These separators assume different states of hardening and softening along their sliding path. The pattern of displacement changes over time is approximately harmonic sinusoidal. The numerical results of the separator modeling can be seen in Table 2. Fig. 7 shows a comparison of the behavior of a separator with a constant radius (R=1000 *mm*) and separators with variable radii based on the elliptic equation.

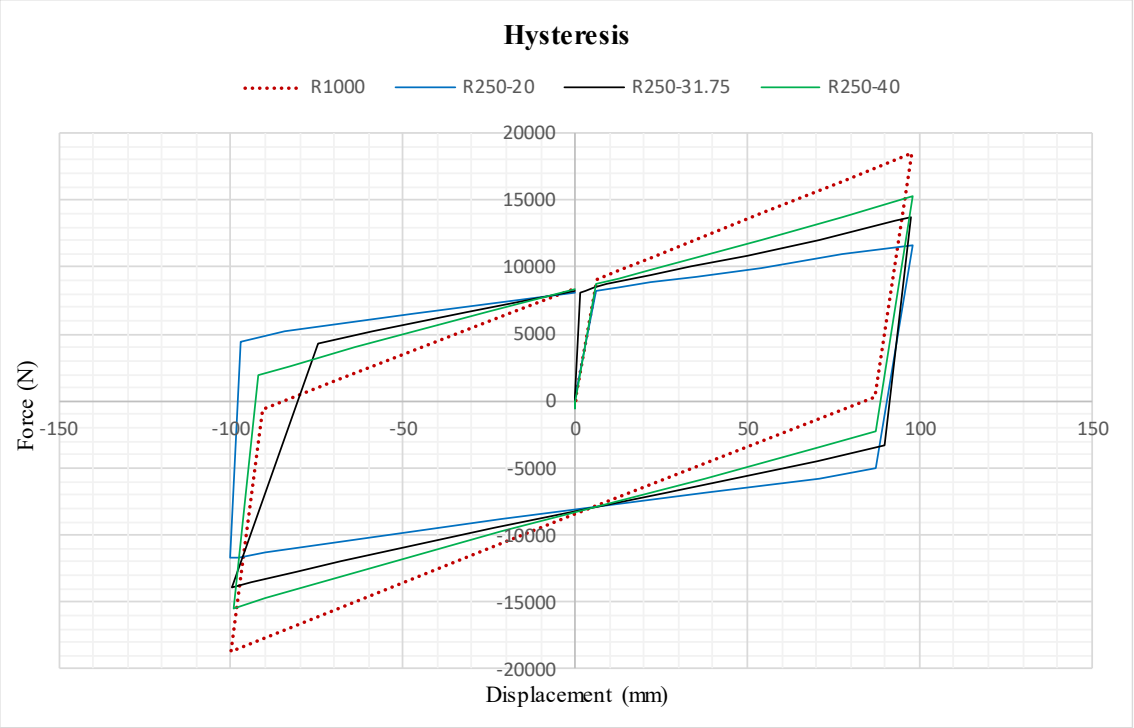

Figure 7: Variable radius separator behavior cycle diagram

Table 2: Properties and specifications of materials and used components

Area (*J*)	k_2	k_1	Min disp. (-) (*mm*)	Max disp. (+) (*mm*)	Radius		Isolation type
					b (*mm*)	a (*mm*)	
3086307.74	36.87	1316.8	-99.9929	97.9562	20	250	
2977141	57.2	5118.7	-99.6327	97.4772	31.75	250	Variable
3111559.66	72.216	1425.1	-99.4054	97.9481	40	250	
3174229.75	102.42	1418.6	-99 .8445	97.9616	1000		Constant

5. DYNAMIC ANALYSIS

Regarding the selection of input records, various parameters come into play. There are numerous earthquake databases available for accessing and downloading records, with some of the most significant ones for civil engineers. For the selection of the desired earthquake records, reference has been made to the Building Design Code for Earthquakes, Standard 2800 [8]. Given the specific consideration for firm and substantial soil conditions, the criteria outlined in Standard 2800 have guided the selection process. One of the crucial parameters is the shear wave velocity, the value of which must fall within the range of 375 to 750 (*m/sec*) for firm soils and exceed 750 (*m/sec*) for very firm soils [8].

By referring to FEMA P695, earthquake records of interest can be selected based on the specified parameters. This allows for the extraction of information such as the earthquake's occurrence location, magnitude, epicenter, and other relevant details [9].

Utilizing the Seismosignal software, a product of Seismosoft, proves to be advantageous in this context due to its user-friendly interface and desirable capabilities. By selecting the desired earthquake records and extracting information for each record in accordance with FEMA P695 guidelines [9], each earthquake record is introduced as input to the Seismosignal software. The specific parameters of each record have been extracted and documented in Table 3.

Table 3. The extracted information from the selected earthquake records

Name	Year	Total time (*Sec*)	Magnitude	Type	Arias intensity (m/sec)
Manjil Iran	1990	53.52	7.4	Far-filed	4.64
Loma Prieta	1989	25.005	6.9	Near-filed	5.36
Northridge-01	1994	47.785	6.7	Near-filed	4.71

By selecting earthquake records and obtaining the characteristics of each record, the spectra of the records can be determined according to Eurocode 8 (EN 1998-1). Fig. 8 illustrates the classification of soil types based on the obtained data [10].

By selecting earthquake records, it is possible to plot the spectrum of records for attenuations of 1%, 5%, and 10%, and by considering the clauses of the Eurocode 8 (EN 1998-1) code, Fig. 8 is obtained, which shows that the selected earthquake records correspond to attenuations of 1%, 5%, and 10% within the accepted periodicity range of the code.

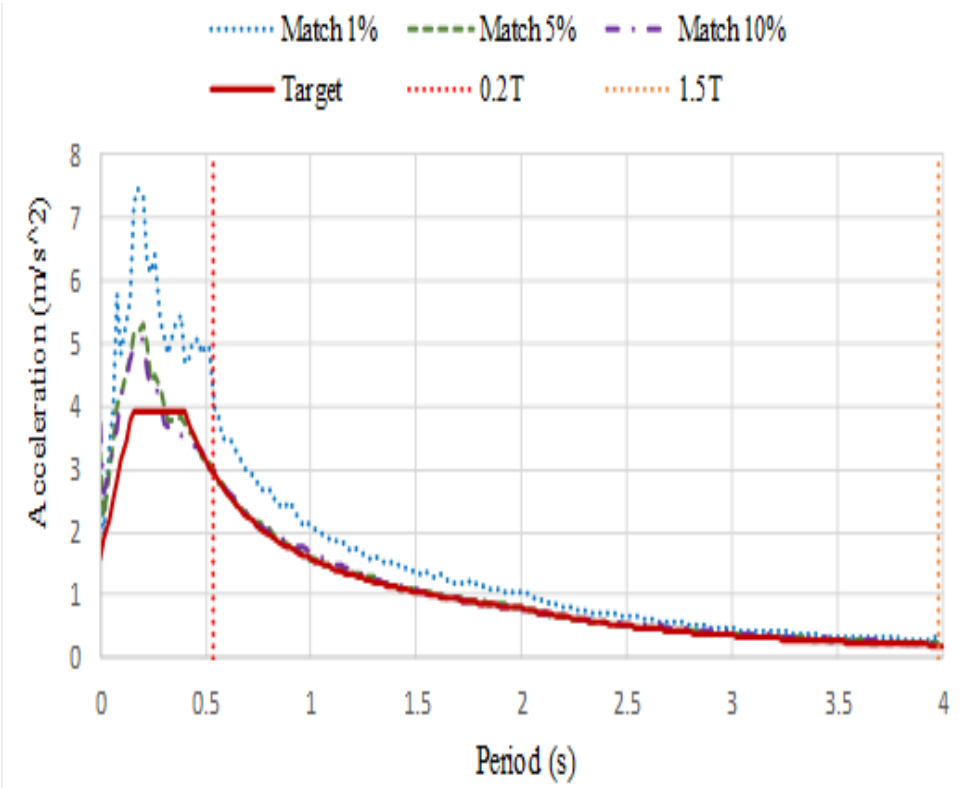

Figure 8: The spectrum diagram of earthquake records for damping ratios of 1%, 5%, and 10%

The spectrum diagram of earthquake records, as per Eurocode 8, is similar to the one specified in Standard 2800 [8]. Considering the seismic isolation period and adhering to the provisions of Standard 2800 [8], as stated below:

- Each pair of acceleration records should be scaled in a way that, for each period within the range of 0.2T to 1.5T (where T is the fundamental period of the structure), the average value of the square root of the sum of squares of all component pairs should not be less than 10% of 1/3 times the corresponding value of the standard design spectrum.

According to the above provision, the standard period has been considered for accessing the spectrum of selected earthquake records, and the results are obtained in accordance with Fig. 7.

Considering the spectrum diagram of the selected earthquake records corresponding to damping ratios of 1%, 5%, and 10% within the acceptable range of the design spectrum (Fig. 8) according to the code, the obtained results are deemed acceptable.

5.1. Majil earthquake

Among the earthquake records investigated in the previous section, seismic records ranging from the Manjil earthquake, the Loma Prieta earthquake, and the Northridge-01 earthquake have been selected here to perform the dynamic analysis. These records are applied in both horizontal directions and on fixed and variable-radius base isolators with an elliptical base. The output results are then compared and evaluated. Fig. 9 shows the displacement time history for the isolator with fixed and variable radius in the x- and y-directions subjected to the Manjil earthquake. Also, Fig. 10 depicts the force-displacement diagram for the *x*- and *y*-directions.

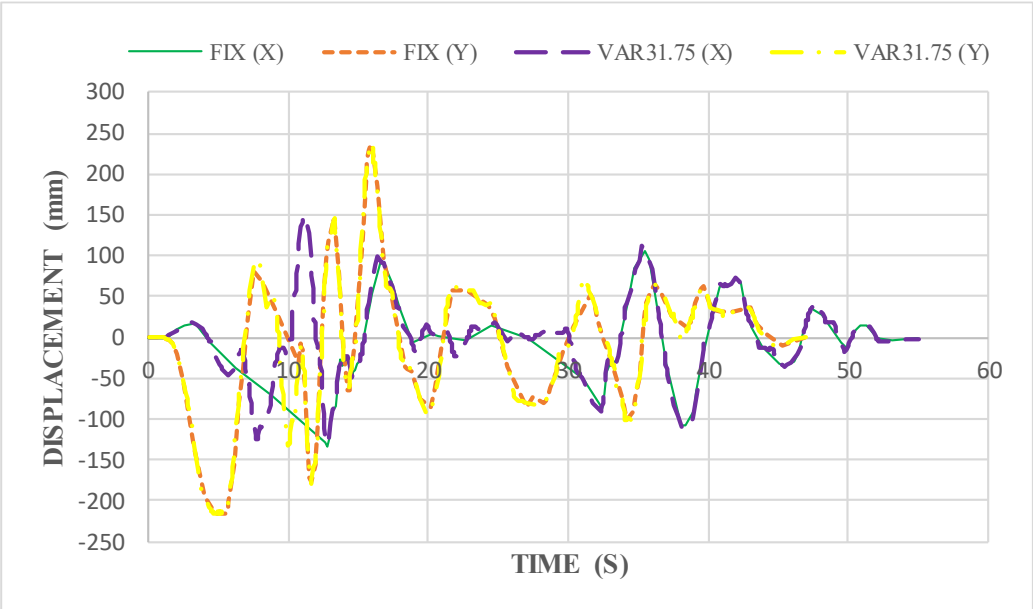

Figure 9: A comparison between the displacement values in both *x* and *y* directions

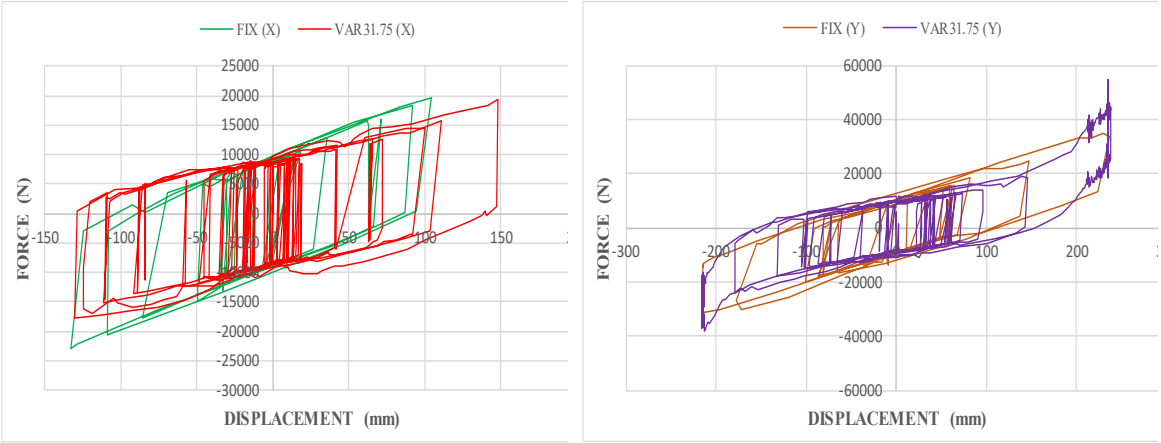

Figure 10: Force-displacement diagram for the *x* and *y* directions

5.2. Loma Prieta earthquake

Fig. 11 shows the displacement time history for the isolator with fixed and variable radius in the x- and y-directions subjected to the Loma Prieta earthquake. Also, Fig. 12 depicts the force-displacement diagram for the *x*- and *y*-directions.

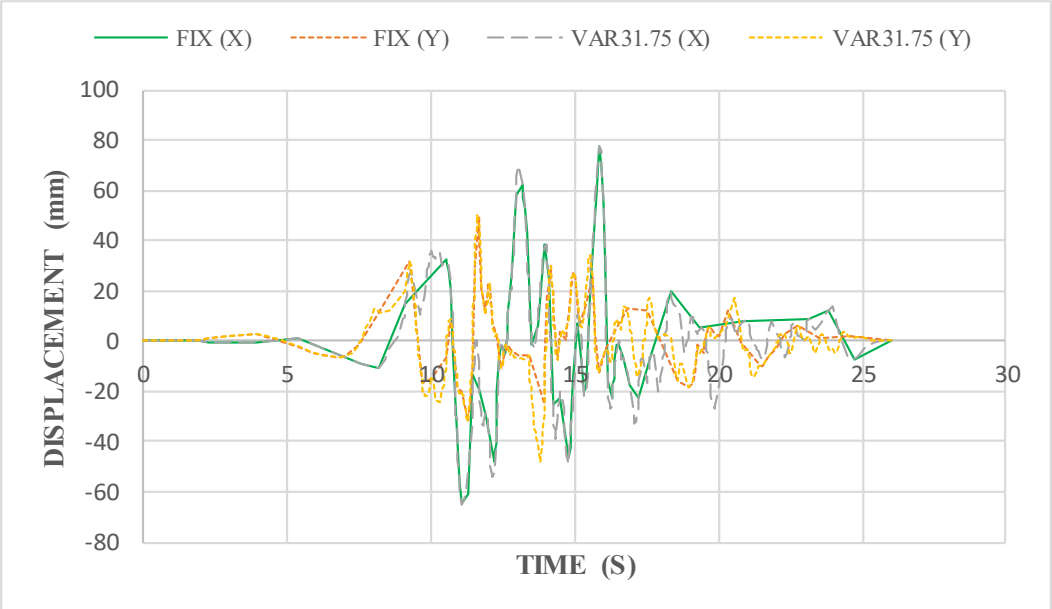

Figure 11: A Comparison between displacement values in both *x* and *y* directions

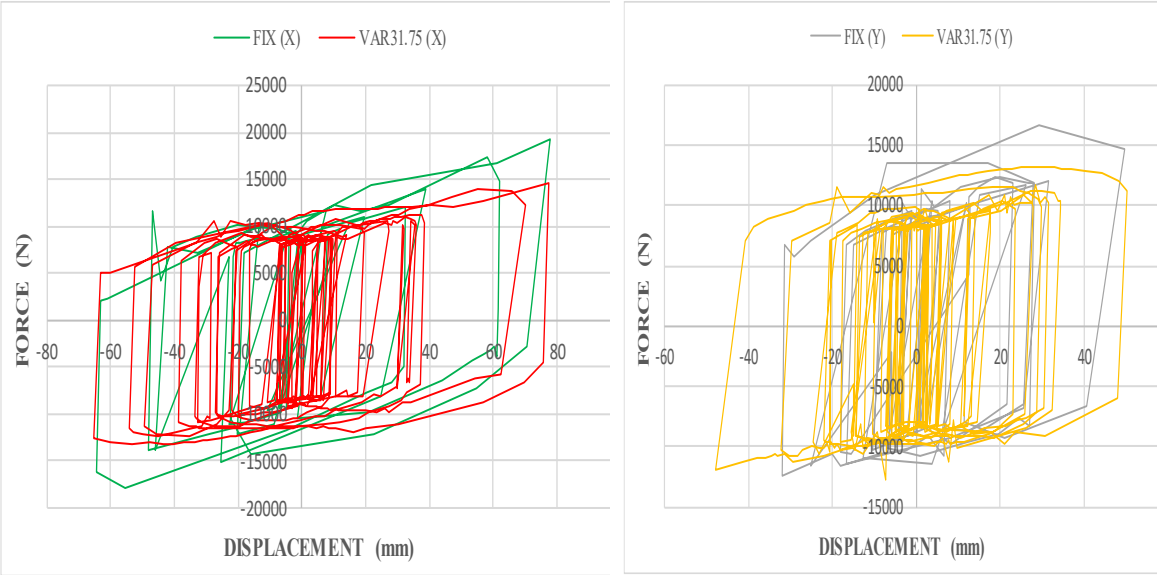

Figure 12: Force-displacement diagram in the x and y directions

5.3. Northridge earthquake

Fig. 13 shows the displacement time history for the isolator with fixed and variable radius in the x- and y-directions subjected to the Northridge earthquake. Also, Fig. 14 depicts the force-displacement diagram for the *x*- and *y*-directions.

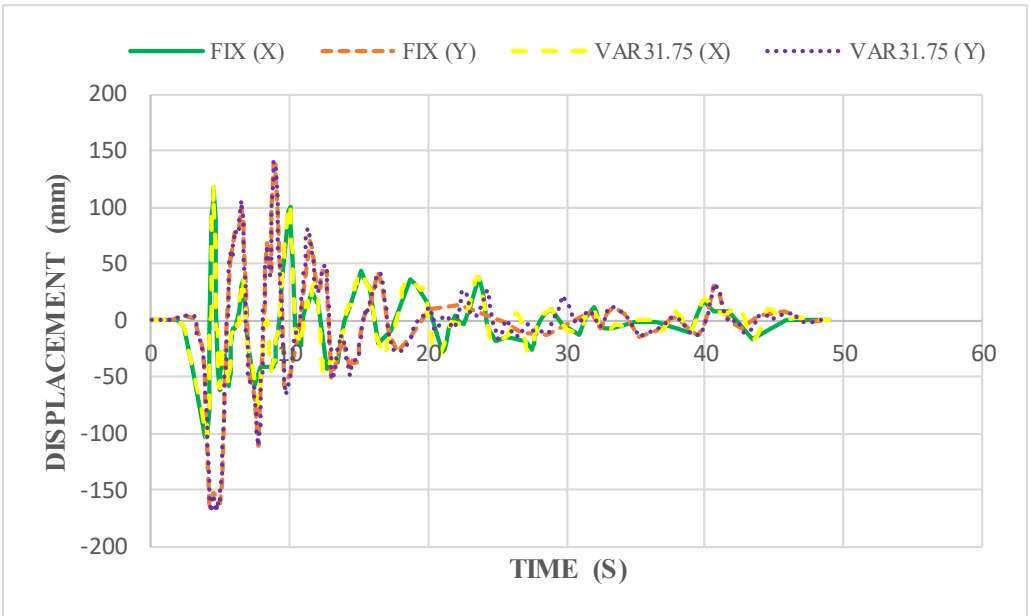

Figure 13: A comparison between the displacement values in both *x* and *y* directions

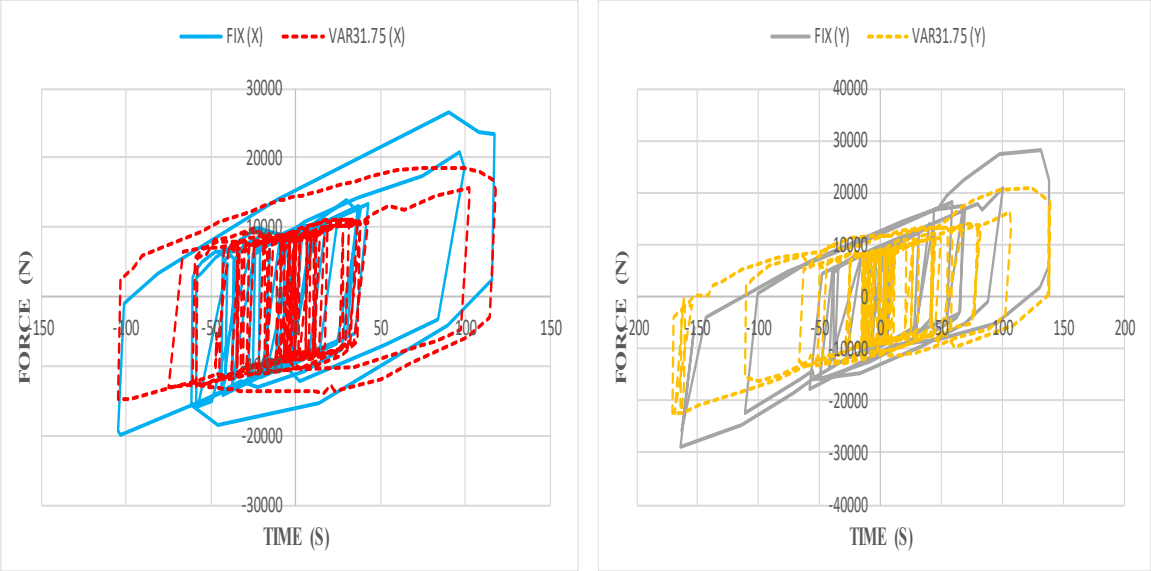

Figure 14: Force-displacement diagram in the *x* and *y* directions

6. NUMERICAL RESULTS

Based on the results obtained from the previous section, the numerical results obtained from the analysis of the output data and the application of earthquake records on fixed-base isolators with a radius of 1000 *mm* and variable-radius base isolators based on an elliptical shape with a major radius of 250 *mm* and minor radii of 31.75 *mm* are as follows (see Tables 4-5). Tables (4-5) display the maximum positive and negative displacements for the four examples of friction pendulum isolators under the influence of earthquake records in both the *x* and *y* directions.

Table 4: The maximum displacement of isolators in the positive direction

Maximum displacement (+) (mm)						**b**	**Type**
Northridge		Loma perieta		Manjil			
y	*x*	*y*	*x*	*y*	*x*		
138.708	116.901	49.699	77.8298	236.709	104.631	1000	Fix
139.452	118.293	50.4215	77.4071	237.999	148.16	31.75	Variable

Table 5: The maximum displacement of isolators in the negative direction

Maximum displacement (-) (mm)						**b**	**Type**
Northridge		Loma perieta		Manjil			
y	*x*	*y*	*x*	*y*	*x*		
164.457	104.494	31.9748	64.32	215.456	133.393	1000	Fix
170.492	104.532	47.9585	65.1246	216.021	130.372	31.75	Variable

The results show that the fixed-radius isolator with a constant radius of 1000 *mm* has lower displacement values compared to the variable-radius isolators. Additionally, it is noted

that reducing the parameter "*b*" (i.e., the minor radius of the ellipse) leads to a decrease in displacement value. Therefore, it can be concluded that the isolators with smaller and more flexible radii demonstrate better capability in reducing earthquake-induced displacements, preventing severe damage [11, 12]. Table 6 shows the energy absorbers by the isolators.

Table 6: Energy absorption capacity of isolators in the face of earthquake records

Energy absorption (kj)						**b**	**Type**
Northridge		Loma perieta		Manjil			
y	*x*	*y*	*x*	*y*	*x*		
18967092	16838589	5524767.8	8331058.2	28515424	12934451	1000	Fix
22040668	19737311	8311493.7	12661867	31821354	21854174	31.75	Variable

It can be concluded that friction pendulum isolators with a variable radius based on an elliptical shape have a higher energy absorption capacity compared to isolators with a constant radius. This suggests that in isolators with a variable radius, the deformability of the system increases with the reduction of parameter "*b*". Therefore, these isolators can absorb more energy and prevent severe damage to the structure. In contrast, isolators with a constant radius, due to their lack of flexibility, have a more limited capability to absorb energy. Consequently, they are more prone to damage and failure under severe seismic loads. Therefore, the results reveal that isolators with a variable radius exhibit higher energy absorption capacities, aligning with the provided explanations.

7. CONCLUSION

Comparison of the results between isolators with constant and variable radii indicates the superior performance of isolators with variable radii. This conclusion is drawn as the optimal and maximum values in isolators with variable radii are greater than those in constant radius isolators. Additionally, the initial and secondary stiffness values (i.e., k_1 and k_2) in isolators with variable radii are higher than those in constant radius isolators, indicating better performance in absorbing energy. The area under the hysteresis curve is also greater in isolators with variable radii, highlighting their higher capability in energy dissipation.

Therefore, it can be inferred that the utilization of friction pendulum isolators with variable radii with the optimum parameters can lead to better performance, particularly in terms of enhanced energy dissipation during seismic events.

8. ACKNOWLEDGMENTS

The authors would like to show their appreciation to the HPC center (Shahr-e-Kord University, Iran) for their collaboration in offering computational clusters, which was a great help in completing this work.

REFERENCES

1. Naeim F, Kelly JM. *Design of Seismic Isolated Structures: From Theory to Practice*. John Wiley & Sons; 1999.
2. Kaveh A, Fahimi Farzam M, Hojat Jalali H. Statistical seismic performance assessment of tuned mass damper inerter. *Struct Control Health Monit*. 2020;**27**(10):e2602.
3. Kaveh A, Javadi SM, Mahdipour Moghanni R. Optimal structural control of tall buildings using tuned mass dampers via chaotic optimization algorithm. *Structures*. 2020;**28**:2704–13.
4. Talatahari S, Kaveh A, Mohajer Rahbari N. Parameter identification of Bouc-Wen model for MR fluid dampers using adaptive charged system search optimization. *J Mech Sci Technol*. 2012;**26**(8):2523–34.
5. Wang L, et al. Friction-based seismic isolation systems: a comparative study. *J Earthq Eng*. 2015;**30**(2):245–63.
6. Fenz DM, Constantinou MC. Mechanical behavior of multi-spherical sliding bearings. University at Buffalo, The State University of New York; 2008.
7. Pranesh M, Sinha R. VFPI: an isolation device for aseismic design. *Earthq Eng Struct Dyn*. 2000;**29**(5):603–27.
8. Iran Institute of Standards and Industrial Research. *Seismic Design Code for Buildings, Standard 2800*. 4th ed. 2014.
9. FEMA-P-695. *Quantification of Building Seismic Performance Factors*. Applied Technology Council, US Department of Homeland Security, FEMA; 2009.
10. Eurocode 8. *Design of Structures for Earthquake Resistance*. British Standards; 2005:1998-1.
11. Jangid RS, Datta TK. Seismic behaviour of base-isolated buildings: a state-of-the-art review. *Proc Inst Civ Eng Struct Build*. 1995;**110**(2):186–203.
12. Makris N, Chang SP. Effect of viscous, viscoplastic and friction damping on the response of seismic isolated structures. *Earthq Eng Struct Dyn*. 2000;**29**(1):85–107.